DESIGN METHODOLOGY OF URBAN AIR MOBILITY FOR NOISE MITIGATION AT CONCEPTUAL DESIGN STAGE

Hojin Kim[1], Donguk Lee[1], Juen Seo[1], Yoonpyo Hong[1], Kwanjung Yee[1*]

[1]Dept. of Aerospace Engineering
Seoul National University, Seoul, Republic of Korea
rhrhak96@snu.ac.kr / oak600p@snu.ac.kr / jueen119@snu.ac.kr / hyp1227@snu.ac.kr / kjyee@snu.ac.kr

Abstract
This article proposes a design methodology for UAM vehicles for noise mitigation at a conceptual design stage. A rotor analysis module for accurate noise prediction and a noise prediction module for a conceptual design stage are constructed. The rotor analysis module is developed for accurately predicting aerodynamic force distribution around rotor blades, thus enabling accurate noise prediction. This module consists of rotor analysis using BEMT or BET methods and CAMRAD II, and these methods exchange force distribution data, which is iterated in the module until aerodynamic force distribution by each method converges. The noise prediction module for a conceptual design stage uses compact loading assumption and dual compact loading assumption, therefore loading and thickness noise prediction are completed in a short time. The proposed design methodology is applied to a conceptual design of an eVTOL aircraft with the lift+cruise concept. Through the design optimization process, the necessity of considering noise impact at the conceptual design stage is demonstrated.

NOMENCLATURE

$E_{\mathrm{on,off}}$	Turn-on and turn-off energies
f_{S}	Switching frequency
G	Change in the slope of the discharge curve due to current
$I_{\mathrm{d,q}}$	d- and q-axis current
I_{ref}	Reference current which is the on-state current after the commutation
I_s	Current space vector
I_{sm}	Voltage space vector
K	Primary dependency of voltage on the capacity discharged
$L_{\mathrm{d,q}}$	d- and q-axis inductance
M	Modulation index
MTOW	Maximum take-off gross weight
N	Number of the battery cell
P	Power
P_{Cu}	Copper loss
P_{Fe}	Iron loss
P_{lc}	Conduction loss
P_{ls}	Switching loss
$P_{\mathrm{no-load}}$	No-load power
P_{p}	Number of pole-pair
Q	Total capacity discharged up to the present instant
R	Internal resistance of the battery cell
R_{ce}	IGBT's differential resistance
R_{F}	Diode's differential resistance
R_{s}	Phase resistance
SP	Specific power
T	Torque
V_0	Open circuit (no load) voltage
V_{ce}	IGBT's threshold voltage
$V_{\mathrm{d,q}}$	d- and q-axis voltage
V_{DC}	DC link voltage
V_{F}	Diode's threshold voltage
V_{ref}	Reference voltage which is the blocking state voltage of the IGBT before the commutation
V_s	Voltage space vector
V_{sm}	Voltage constraint
β	Phase angle
η	Efficiency
λ_0	Stator permanent magnet flux linkage
ω_{b}	Base speed
ω_{e}	Electrical velocity

1. INTRODUCTION

Since Uber announced their first vision for future mobility industry in 2016 [1], interest in urban air mobility (UAM) with electric vertical take-off and landing (eVTOL) concept has increased. The advancements in electrification, automation, and VTOL further increase interest and accelerate the emergence of eVTOL aircraft. eVTOL aircraft is considered as the most suitable type for UAM because it causes no emission problem which is serious in modern cities such as New York and Seoul [2]. In addition, it is capable of VTOL, which is essential in urban areas without proper runways [3].

However, a rotary wing system used in VTOL aircraft makes large noise by nature and causes people to get diseases such as hearing loss and insomnia if they are continuously exposed to that noise [4]. Therefore, except for medical use, communities have opposed other uses of UAM on-demand services due to their noise [1]. In addition,

national institutions such as Federal Aviation Administration (FAA) and International Civil Aviation Organization (ICAO) have set criteria for VTOL aircraft designs and operations for low noise impact on communities [5]. For that reason, noise impacts of eVTOL aircraft should be considered as one of the most important issues along with safety and eco-friendliness for the prosperity of the UAM industry.

Meanwhile, because of the large noise characteristics of VTOL aircraft with a rotary wing system, much research has been conducted on reducing aeroacoustic noise from the rotary wing system. Chae. [6] conducted design optimization of a rotor blade, where UH-1H rotor blade was set as the baseline blade. Acoustic pressure peak and power coefficient at the hovering condition are set as objective functions and total 17 design variables were used in the design optimization, where 13 of them are related with blade planform design and the others are related with airfoil design. Hong. [7] carried out parametric study of a drone blade design with wavy leading edges on the aeroacoustic performance. Three design variables are used in the parametric study, and those variables are horizontal wave amplitude, vertical wave amplitude and sweep factor.

However, according to Fualkner, a new tip planform and twist distribution of a rotor blade can reduce noise to some degree but cannot reduce it dramatically [8]. Instead, noise mitigation effect by rotor tip speed reduction is much larger than that by the new planform design and twist distribution of the rotor blade. In spite of the fact that the rotor tip speed plays the most important role in reducing noise, the aforementioned research [6,7] only carried out planform and twist design optimization for aeroacoustic performance under the fixed blade tip speed. This is because conventional helicopters with engines have very limited range of rotational speed, therefore rotor tip speed is almost fixed.

On the other hand, VTOL aircraft with electric motors have a wider range of rotation speed than that with engines, thus suggesting that the tip speed should be considered as one of design variables when we design a rotor blade for eVTOL aircraft. And since the rotor tip speed of eVTOL aircraft is determined at a conceptual design stage where electric propulsion system (EPS) sizing is carried out, it can be suggested that noise prediction and mitigation of eVTOL aircraft should be conducted at the conceptual design stage.

Our Primary objective in this paper is providing a new framework for noise prediction and mitigation at a conceptual design stage of eVTOL aircraft. For a conceptual design of eVTOL aircraft, we use RISPECT+ (Rotorcraft Initial Sizing and Performance Estimation Code and Toolkit+) program, which is developed for sizing and performance analysis of various VTOL aircraft and provides EPS analysis modules. In the previous version of RISPECT+, blade element momentum theory (BEMT) and blade element theory (BET) are used for flight analysis since these methods are able to quickly estimate thrust and required power made by each rotor at the conceptual design stage. However, these methods are not suitable for accurate noise prediction, which requires accurate flow field prediction around rotor blades. In addition, these methods assume that there is no aerodynamic interaction between each rotor, which can cause inaccurate performance analysis and noise prediction for eVTOL aircraft with many rotors which are close to each other. Therefore, a comprehensive analytical model of rotorcraft aerodynamics and dynamics II (CAMRAD II) [9] is used for accurately predicting aerodynamic force distribution around rotor blades under rotor-rotor aerodynamic interaction. On top of that, since the general forms of Farassat's 1A loading and thickness noise formula require surface integral for noise sources, constructing blade surface grids are necessary [16]. For this reason, the loading noise formula with compact loading assumption and the thickness noise formula with dual compact loading assumption are used in this study. Therefore, fast noise prediction at the conceptual design stage is possible.

The remainder of this paper is organized as follows. Section 2 briefly introduces overall flow of RISPECT+. Section 3 and 4 details the four sizing modules in RISPECT+ and the noise analysis module respectively. Section 5 presents parametric study results of an eVTOL aircraft using the proposed framework. Section 6 provides optimization result of the eVTOL aircraft. Finally, Section 7 discuss the results and provides conclusion of the paper.

2. CONCEPTUAL DESIGN FRAMEWORK FOR EVTOL AIRCRAFT: RISPECT+

In this study, the conceptual design framework RISPECT+ [10] (Rotorcraft Initial Sizing and Performance Estimation Code and Toolkit+) is used. RISPECT+ was developed as a program to provide performance analysis and initial sizing results for VTOL aircraft with various kinds of configurations. It also provides EPS analysis modules, therefore accurate weight estimation of

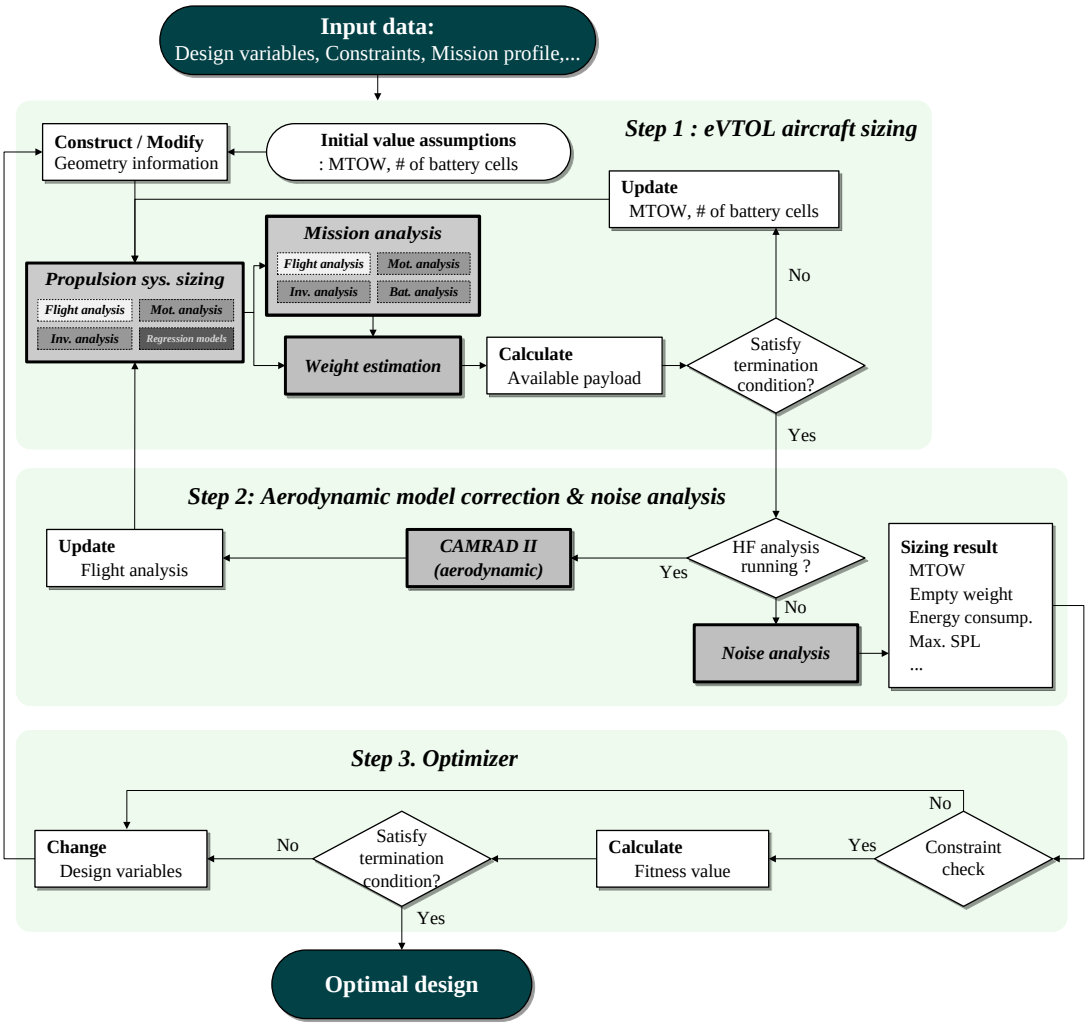

Figure 1 Overall Flow Chart of RISPECT+

EPS for eVTOL aircraft is possible [11]. As in Figure 1, RISPECT+ consists three stpes. In step one, initial sizing of an eVTOL aircraft using input design conditions is conducted. Modules in this step consist of 1) flight analysis module, 2) propulsion system sizing module, 3) mission analysis module and 4) weight estimation module. In step two, aerodynamic model correction and noise analysis are conducted. In this step, by coupling the flight analysis module in RISPECT+ and CAMRAD II, accurate aerodynamic force calculation is conducted. In addition, by using the newly developed noise prediction module, noise impact of each eVTOL aircraft is evaluated. In step 3, by calculating each design's fitness, design optimization is coudcted. Overall flow of RISPECT+ with noise prediction is in Fig. 1.

3. SIZING MODULE IN RISPECT +

Sizing modules in RISPECT+ consist of flight analysis module, propulsion system sizing module, mission analysis module and weight estimation module. Each module is explained in this section.

3.1. Flight analysis module

As mentioned above, the previous version of RISPECT+ uses BEMT and BET methods for fast estimation of rotor performance at a conceptual design stage[]. These methods can be considered as suitable if calculating rotor performance and conducting initial weight estimation of eVTOL aircraft are the only interests at the conceptual design stage. However, with respect to accurately predicting noise impacts caused by multiple rotors, these methods are not proper because they assume that there is no aerodynamic interaction between each rotor, therefore neglecting aerodynamic force distribution change around rotor blades due to the rotor-rotor interaction effect. Specifically, BEMT method calculates the inflow ratio, $\boldsymbol{\lambda_i}$ across the radial direction of the rotor blade and determines lift coefficient, $\boldsymbol{C_l}$ and drag coefficient, $\boldsymbol{C_d}$ at each blade section, assuming that there is no rotor-rotor interaction. Therefore, all

rotors have the same rotational speed and C_l and C_d distribution. However, when more than two rotors are under rotor-rotor interaction, the aerodynamic force distribution is influenced by the interaction. Therefore, noise source generation is affected by the interaction. [3]

For this reason, in this study, RISPECT+ & CAMRAD II coupling is used for accurately predicting aerodynamic force distribution around rotor blades under rotor-rotor interaction. The flow chart of RISPECT+ & CAMRAD II coupling is in Fig. 2.

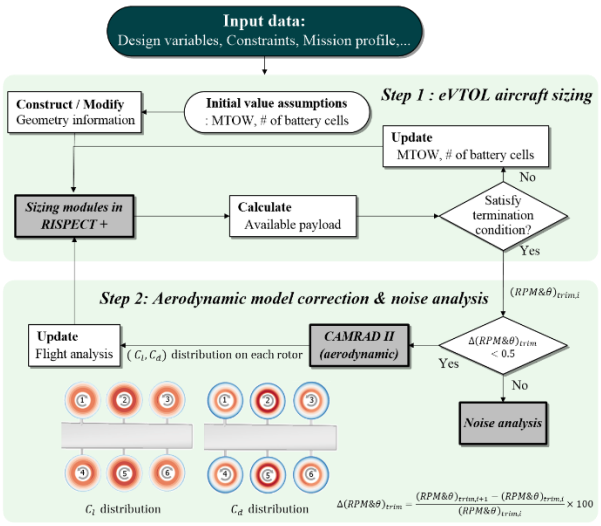

Figure 2 RISPECT+ & CAMRAD II Coupling

First, for a given set of input design variables, RISPECT+ conducts initial sizing for an eVTOL aircraft as seen in Fig. 2. In this process, RISPECT+ only uses BEMT / BET methods for predicting aerodynamic force distribution around rotor and propeller blades and calculates control input sets of rotors and propellers for a trimmed condition at each mission segment. Then, the control input sets at each mission segment are provided to CAMRAD II as input operating conditions ,and aerodynamic force distribution around rotor and propeller blades are caculated using the free wake model. Now the force distribution at each rotor and propeller blade obtained by CAMRAD II is provided to RISPECT+, and RISPECT+ conducts flight analysis modified by the force distribution and resizes the eVTOL aircraft. In this sizing process, RISPECT+ again calculates control input sets of rotors and propellers for a trimmed condition, and they are used again by CAMRAD II as input operating conditions. This procedure repeats until the difference of control inputs for a trimmed condition between present and previous step is less than 1%.

After the procedure ends, final gross weight of the eVTOL aircraft is determined and noise analysis module calculates noise impacts of the eVTOL aircraft. Figure 3 shows the process where C_l and C_d distributions calculated by RISPECT+ and CAMRAD II converge to each other.

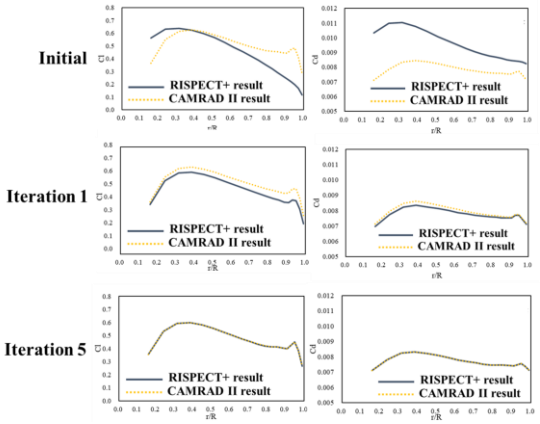

Figure 3 Convergence History of RISPECT+ & CAMRAD II Coupling

3.2. Electric propulsion system sizing module

3.2.1 Motor analysis

For the analysis of the permanent magnet synchronous motor (PMSM), three control strategies that can help an efficient operation of the PMSM are utilized in this study, and they are described below [12].

Maximum torque per ampere (MTPA) control: This concept is a control method to obtain the maximum torque under the given stator current amplitude by controlling d- and q- axis current components.

Field weakening or Maximum torque per voltage control: These concepts increase the rotational speed by reducing electromagnetic torque. Because propulsive loads (fan, rotor, or propeller) reach high power and high speed simultaneously, field weakening and maximum torque per voltage control strategies to achieve high speed at the expense of torque are not useful for aircraft propulsion.

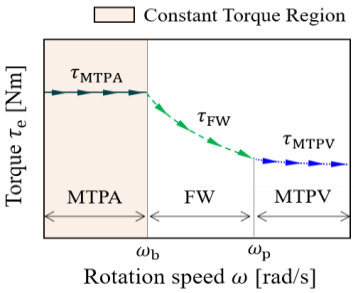

Figure 4 Example of the PMSM Control Using Three Control Strategies

Figure 4 shows an example of the PMSM control using three control strategies mentioned above and Figure 5 shows the input current vector trajectory at control strategy for efficient operation of the PMSM.

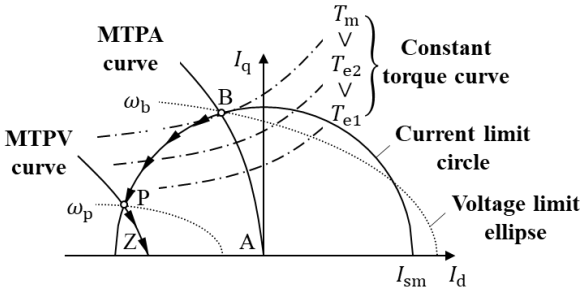

Figure 3 Input Current Vector Trajectory

As it can be seen in Figure 4, which type of control strategy will be used basically depends on the torque and corresponding rotational speed of motor. Therefore, baseline speed $\boldsymbol{\omega_b}$ and critical speed $\boldsymbol{\omega_p}$ should be obtained first to determine a control startegy at a given torque and rotational speed.

Electromagnetic torque $\boldsymbol{T_e}$ can be obtained by using Eq. (1)

$$(1)\ \boldsymbol{T_e} = \frac{3}{2}\frac{P}{2}\left[\lambda_0 I_q + \left(L_d - L_q\right) I_d I_q\right]$$
$$= \frac{3}{2}\frac{P}{2}\left[\lambda_0 I_s sin\beta + \frac{\left(L_d - L_q\right)}{2} I_s sin2\beta\right]$$

And by differentiating equation (1) with respect to the phase angle $\boldsymbol{\beta}$, the optimal d- and q- axis current components that maximize $\boldsymbol{T_e}$ can be calcuated. The optimized curruent component of each axis are in Eqs. (2) and (3)

$$(2)\ \boldsymbol{I_{dm}} = \frac{\lambda_0}{2(L_q - L_d)} - \sqrt{\frac{\lambda_0}{16(L_q - L_d)^2} + \frac{I_{sm}^2}{2}}$$

$$(3)\ \boldsymbol{I_{qm}} = \sqrt{I_{sm}^2 - I_{dm}^2}$$

In addition, the baseline speed $\boldsymbol{\omega_b}$ until which the PMSM can maintain maximum torque under current limit and voltage limit can be obtained by using Eq. (4). And as it can be seen in Figure 4, the limiting point for MTPA control is where MTPA curve, current limit curve and voltage limit curve cross.

$$(4)\ \boldsymbol{\omega_b} = \frac{V_{sm}}{\sqrt{\left(L_d I_{dm} + \lambda_0\right)^2 + \left(L_q I_{qm}\right)^2}}$$

If motor speed of the PMSM becomes larger than $\boldsymbol{\omega_b}$, the PMSM applies FW control under the given voltage limit condition. Since maximum terminal volatge becomes smaller as motor speed becomes larger, allowable torque decreases with the increase of motor speed. Current component of d- and q- axis under FW control can be determined by using Eqs. (5) and (6)

$$(5)\ \boldsymbol{I_{dn}} = -\frac{-2L_d\lambda_0 + \sqrt{(2L_d\lambda_0)^2 - 4\left(L_d^2 - L_q^2\right)\left(\lambda_0^2 + L_q^2 I_m^2 - \left(\frac{V_m}{\omega_e}\right)\right)}}{2\left(L_d^2 - L_q^2\right)}$$

$$(6)\ \boldsymbol{I_{qn}} = \sqrt{I_{sm}^2 - I_{dn}^2}$$

When the motor speed increases until critical speed $\boldsymbol{\omega_p}$, FW control is the best strategy for providing the largest torque. However, if the motor speed becomes larger than $\boldsymbol{\omega_p}$, the PMSM can provide higher torque by using MTPV control than FW control. The critical speed $\boldsymbol{\omega_p}$ can be obtained by equating the torque produced by FW $\boldsymbol{T_n}$ and the torque produced by MTPV control $\boldsymbol{T_p}$ and finding the $\boldsymbol{\omega_p}$ that satisfies that equation. $\boldsymbol{T_n}$ can be calcualted by Eqs. (1), (5) and (6); $\boldsymbol{T_p}$ can be calculated by Eqs. (1), (7), (8) and (9).

$$(7)\ \boldsymbol{I_{dp}} = -\frac{\lambda_0}{L_d} - \Delta\boldsymbol{I_d}$$

$$(8)\ \boldsymbol{I_{qp}} = \frac{\sqrt{\left(V_{sm}/\omega_e\right)^2 - \left(\Delta I_d L_d\right)^2}}{L_q}$$

$$(9)\ \Delta\boldsymbol{I_d} = \frac{\frac{L_q}{L_d}\lambda_0 + \sqrt{\left(\frac{L_q}{L_d}\lambda_0\right)^2 + 8\left(\frac{L_q}{L_d} - 1\right)^2\left(\frac{V_{sm}}{\omega_e}\right)}}{4\left(L_d - L_q\right)}$$

After obtaining $\boldsymbol{\omega_b}$ and $\boldsymbol{\omega_p}$, motor efficiency can be calculated as Eq. (10) using the current and voltage component at each operating control strategy and motor parameters determined through motor sizing procedure.

$$(10)\ \boldsymbol{\eta_{motor}} = \frac{P_{mech}}{P_{mech} + P_{iron} + P_{copper} + P_{no-load}}$$

More detailed information about each loss component can be found in [16].

3.2.2 Inverter analysis

In this study, inverters with six pairs of insulated gate bipolar transistor (IGBT) and diode are used for calculating inverter efficiency.

For the inverter composed of pairs of IGBT and diode, power loss by the inverter, $\boldsymbol{P_{loss,inv}}$ can be obtained by the sum of switching loss, $\boldsymbol{P_{ls}}$ and conduction loss, $\boldsymbol{P_{lc}}$ and they are calculated as in [13, 14]

$$(16)\ \boldsymbol{P_{loss,inv}} = 6 \times \left(\boldsymbol{P_{ls}} + \boldsymbol{P_{lc,I}} + \boldsymbol{P_{lc,D}}\right)$$

Since input voltage and current of motor and output voltage of battery are needed for calculating power

loss by the inverter. Therefore, motor, inverter and battery analysis should be conducted at every time step among every mission segment.

3.2.3 Battery analysis module

In this study, nearly-linear discharge model is used for battery analysis. Since the model considers output voltage drop effect of battery as discharge undergoes, it can accurately calculate battery cell curruent and voltage and therefore the inverter efficiency and battery depth of discharge (DOD). Mathmatical modeling of battery cell voltage is in Eq. (22) [15] .

$$(22)\quad V = 0.5\left[(V_0 - KQ) + \sqrt{(V_0 - KQ)^2 - 4(RP + GQP)}\right]$$

3.3. Mission analysis module

At mission analysis module, flight analysis explained in Sec. 3.1. is conducted at all mission segements such as take off, hovering and cruising and rotor operation indices such as required power and rotational speed are calculated. Then, by using EPS analysis moudles mentioned in Sec. 3.2., the total discharged battery capacity is calculated and finally the minimum numer of battery cells to satisfy the whole mission profile is determined.

3.4. Weight estimation module

Weight estimation module calculates the weight of each component of eVTOL aircraft such as motor, inverter, wing and fuselage using table data. More detailed information can be found in [16].

4. NOISE PREDICTION IN RISPECT +

In this study, only loding noise and thickness noise are calculated for predicting noise from eVTOL aircraft. Mathmatical modeling of each noise component is described below.

4.1. Loading noise

In this study, Farasst's 1A loading noise formula [17] with compact loading assumption [18] is used for calculating loading noise from rotors. In compact loading assumption, sectional loading is assumed to be applied at $\frac{c}{4}$ of airfoil and that point is used as a noise source for loading noise calculation. By using this assumption, surface integral in original Farassat's 1A loading noise formula changes to line integral as in Eq. (23), therfore flowfield data from comprehensive analysis code can be used for loading noise prediciton and time efficient noise prediction is possible.

$$(23)\ 4\pi p'_L(x,t) = \frac{1}{c}\int_{f=0}\left[\frac{\dot{L_r}}{r|1-M_r|^2}\right]_{ret} dR + \int_{f=0}\left[\frac{L_r - L_M}{r|1-M_r|^2}\right]_{ret} dR + \frac{1}{c}\int_{f=0}\left[\frac{L_r\left(r\dot{M}_r + cM_r - cM^2\right)}{r^2|1-M_r|^3}\right]_{ret} dR$$

4.2. Thickness noise

For calculating thickness noise prediction, Farassat's 1A thickness noise formula with dual compact loading assumption is used in this study [19]. In dual compact loading assumption, all chordwise nosie sources along blade surface are replaced by two loading sources of which loading values are $\rho_0 c_0^2 h$ respectively and directions are opposite to that of each other as in Figure 6. As in compact loading assumption, this assumption can help time efficient calculation of thickness noise. Validations between thickness noise calculated by normal thickness noise formula and dual compact loading assumption are shown in Figure 7.

h: maximum thickness of airfoil

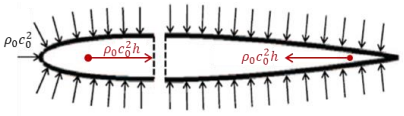

Figure 6 Dual Compact Loading Assumption for Thickness Noise

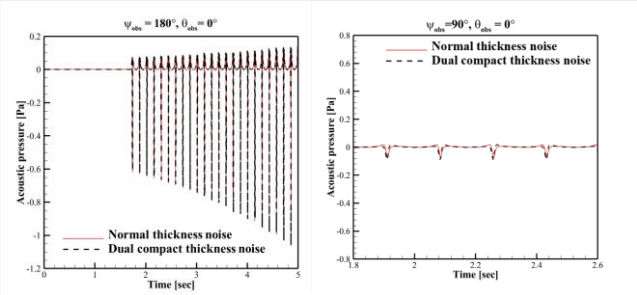

Figure 7 Comparison Between Normal Thickness Noise Formula and Dual Compact Loading Assumption

4.3. Retarded-time algorithm

In this study, as a retarded-time algorithm, soure-time-dominant algorithm was used [20]. In this algorithm source time is regarded as the primary

time (dominant time). For calculating aeroacoustic pressure change at observers, the source time is chosen first and then determine the time when the signal will reach the observer. Next, acoustic pressures are interpolated based on desired observer times.

5. PARAMETRIC STUDY OF AN EVTOL AIRCRAFT DEISGN USING THE FRAMEWORK

Using the proposed framework, parametric study was conducted to see an effect of each design variable on the quantities of interest (QOIs). In this study, QOIs consist of major QOIs such as gross weight and noise impact of an eVTOL aircraft and minor QoIs such as motor weight and hovering tip Mach number.

5.1. Problem definition

Wisk Cora was used as the baseline eVTOL aircraft and its geometric data is in Table 1., and its three-dimensional modeling is in Figure 8. For mission profile of the eVTOL aircraft, simplified version of Uber Elevate mission profile [21] was used as in Figure 9.

Table 1 Geometric Data of Wisk Cora [21]

Rotor[1]	Disk loading (per rotor): 14.76 lb/ft2
	Aspect ratio: 3.17
	Taper ratio: 0.75
	Collective pitch: 13.5 deg
Wing[1]	Wing loading: 19.45 lb/ft2
	Aspect ratio: 12.4
	Taper ratio: 1
Propeller[1]	Radius: 3.5 ft
	Solidity: 0.1

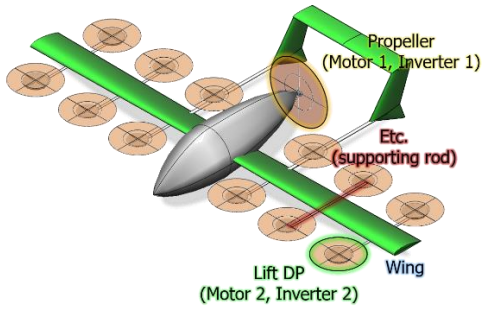

Figure 8 Three-dimensional Modeling of Wisk Cora [10]

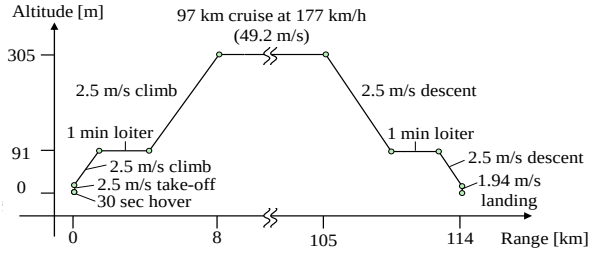

Figure 9 Uber Elevate Mission Profile [21]

For the parametric study, 12 design variables are used, and the target payload of eVTOL aircraft is set as 400 lb. Details about each design variable and payload are listed in Table 2.

Table 2 Design Variables & Payload

DV	**Rotor**			
	Radius [ft]	Chord [ft]	Twist [deg]	Incidence angle [deg]
	$1.8 < R_{rotor} < 2.4$	$0.5 < c_{rotor} < 0.8$	$-15 < \theta_{tw,rotor} < 0$	$13.5 < \theta_{0,rotor} < 23.8$
	Propeller			
	Radius [ft]	Chord [ft]	Twist [deg]	Rotational speed [RPM]
	$3 < R_{prop} < 4.2$	$0.3 < c_{prop} < 0.43$	$-18 < \theta_{tw,prop} < -12$	$1950 < RPM_{prop} < 2640$
	Wing			
	Span [ft]	Aspect ratio	Incidecne angle [deg]	Supporting rod length [ft]
	$32.8 < Span_{wing} < 43.2$	$10 < AR_{wing} < 15$	$10 < \theta_{wing} < 15$	$6.4 < l_{rod} < 9.6$
Payload	400 lb (fixed)			

For assessing the noise impact of each eVTOL aircraft design, the quantitative criteria suggested in Uber Elevate was used. According to Uber Elevate white paper, UAM departing from or landing at vertiports should satisfy noise level criteria that maximum A-weighted overall sound pressure level (OASPL) on the ground, L_{Amax} is approximately 62 dBA at 500ft [1]. Therefore, L_{Amax} on the ground while an eVTOL aircraft is hovering at 500 ft was chosed as an assesment for noise impact of each eVTOL aircraft design. For calculating L_{Amax} , C_l & C_d distribution and rotational speed of each rotor determined through the sizing procedure mentioned in Section 3 are provided to the noise prediction module. Then, using the noise prediction module, acoustic pressure change is calculated at each point on the ground which is 500 ft below an eVTOL aircraft, and A-weighted OASPL is calculated at each point. Finally, L_{Amax} is determined among all points on the ground. For example, noise countour of the baseline eVTOL aircraft is in Figure 10 and calculated L_{Amax} is 74.8 dBA

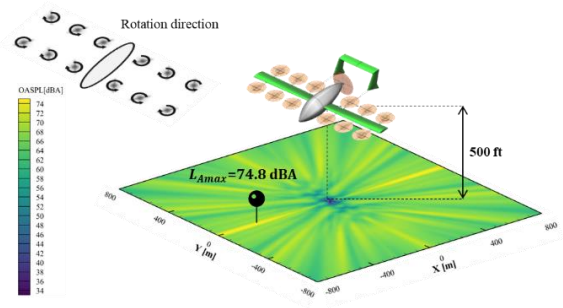

Figure 10 Noise Contour (A-weighted OASPL) of The Baseline eVTOL Aircraft on The Ground

5.2. ANOVA and sensitivity analysis

For conducting analysis of varinace (ANOVA) and sensitivity analysis between design variables and QOIs, a surrogate model was construced using Gaussian Process Regression (GPR) where total 3000 points were sampled through latin hypercube sampling (LHS) [22]. GPR assumes likelihood function as Gaussian and applies posterior Gaussian process for predicting functions [23]. Validation of each GPR model is in Appendix. However, in this sizing problem, not all sets of design variables can satify the target payload even though the sizing moudle in RISPECT+ increases the gross weight to get the payload of 400 lb. For example, if $\boldsymbol{R_{prop}}$ of an eVTOL aircraft gets smaller, a higher propeller collective pitch at the cruising mission is required. And if $\boldsymbol{R_{prop}}$ is too small, the required collective pitch at the cruising mission is too high, and the input collective pitch crosses the limit where stall occurs, showing an unacceptable performance. Finally, the eVTOL aircraft with too small $\boldsymbol{R_{prop}}$ cannot complete the cruising mission, therefore is not capable of satisfying the target payload. For this reason, another surrogate model should be constructed for classifying the whole design space into feasible and infeasible space. For this, we used Gaussian Process Classifier (GPC). GPC uses Laplace approximation for the posterior process because targets are discrete class labels, and is suitable for binary classification or multi-class classification [23]. In this problem, target labels are 'feasible' and 'infeasible', therefore GPC for a binary problem is used. Validation of GPC is in Appendix.

For analyzing relations between design variables and QOIs, Analysis of variance (ANOVA) was performed. ANOVA is a method that quantitatively estimates global sensitivity of each design variable by calculating the ratio of a covariance of a design variable to a total variance of all design variable sets [24]. In this study, ANOVA was performed for two major QOIs, $\boldsymbol{GW}$ and $\boldsymbol{L_{Amax}}$. Furthermore, sensitivity analysis was performed for analyzing relations between design variables and QOIs in more detail. In this analysis, the baseline eVTOL aircraft was chosen as a reference point, and crossings between two red dotted lines mean the reference point. Areas with gray color mean infeasible design spaces that cannot satisfy the target payload, which are classified by the GPC model mentioned above.

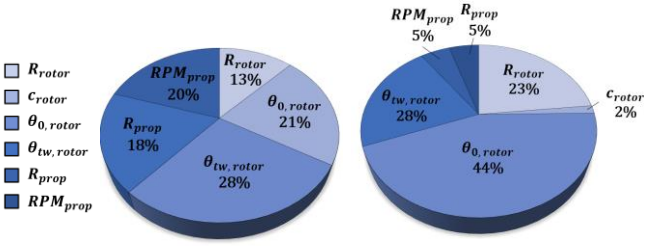

(a) GW (b) L_{Amax}

Figure 11 ANOVA Results

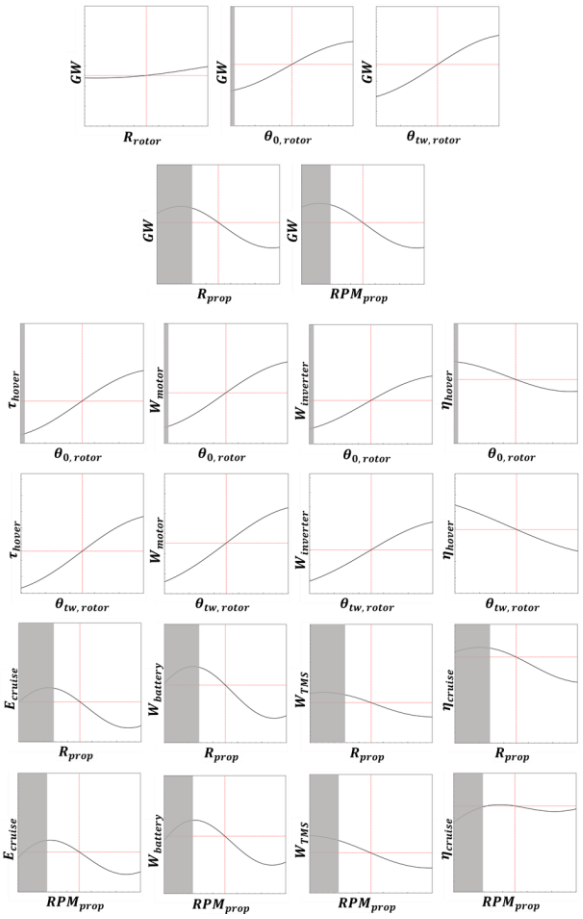

Figure 12 Sensitivity Analysis Results for GW

As in Figure 11., through ANOVA for $\boldsymbol{GW}$, $\boldsymbol{\theta_{0,rotor}}$, $\boldsymbol{\theta_{tw,rotor}}$ and $\boldsymbol{R_{rotor}}$ are identified as having significant effects on $\boldsymbol{GW}$. The reason for their influences is that hovering performance of a rotor

is closely related with the motor size. Maximum required power and torque occur at the hovering mission, and as mentioned in Section 3.2.1, motor sizing is conducted based on the maximum required torque among all mission segments. Therby, the hovering performance is important in deciding the weight of motor. And the weight of other subsystems such as inverters and wiring increases in proportion to the increase of the motor weight. Therefore, $\boldsymbol{\theta_{0,rotor}}$ and $\boldsymbol{\theta_{tw,rotor}}$ that are closely related with hovering performance are influential in determining the gross weight. These relations are confirmed in the sensitivity analysis in Figure 12. As $\boldsymbol{\theta_{0,rotor}}$ increases, the required torque, $\boldsymbol{\tau_{hover}}$, for the hovering mission increases, which leads to the increase of the motor weight, $\boldsymbol{W_{motor}}$. This is accompanied by the weight increase of the inverter, $\boldsymbol{W_{inverter}}$, thus causing the total weight increase. Furthermore, it is shown that the increase of $\boldsymbol{\theta_{0,rotor}}$ corresponds with the decrease of the total system efficiency at the hovering mission, $\boldsymbol{\eta_{hover}}$. This is same for $\boldsymbol{\theta_{tw,rotor}}$ as in Figure 12. In addition, as in Figure 11, $\boldsymbol{R_{prop}}$ and $\boldsymbol{RPM_{prop}}$ are also recognized as important design variables when deciding the gross weight. This is because the weight of battery is closely related with the cruising performance. As mentioned in Section 3.3, the number of parallel and serial battery cells is determined by calculating required energy through whole mission profile. And since the duration of the cruising mission is about 50 minutes, used energy at the cruising mission takes most of the total used energy. For this reason, battery weight is closely related with the cruising performance. And similar with a motor, the weight of other electric propulsion subsystems such as thermal management sysemt (TMS) increases as the weight of the battery increases, design varaibles such as $\boldsymbol{R_{prop}}$ and $\boldsymbol{RPM_{prop}}$ have large impacts on the gross weight. We can validate these correlations in depth by conducting sensitivity analysis. As in Figure 12, as $\boldsymbol{R_{prop}}$ increases, the required energy, $\boldsymbol{E_{cruise}}$, for the cruising mission decreases, thus leading to the increase of the battery weight, $\boldsymbol{W_{battery}}$ and the TMS weight, $\boldsymbol{W_{TMS}}$. But this trend changes to the opossite after a point because as $\boldsymbol{R_{prop}}$ increases, he tip speed of a propeller increases, which is followed by the increase of the required power for the propeller. This is same for $\boldsymbol{RPM_{prop}}$ as in Figure 12.

When ANOVA is conducted for $\boldsymbol{L_{Amax}}$, $\boldsymbol{\theta_{0,rotor}}$, $\boldsymbol{\theta_{tw,rotor}}$ and $\boldsymbol{R_{rotor}}$ are the most influential in deciding the noise impact. This is because the magnitude of aeroacoustic noise from rotors largely depends on the rotor tip speed, which corresponds with Faulkner's research on the

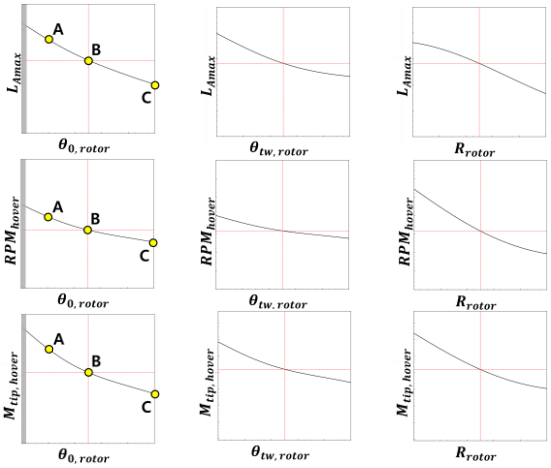

Figure 13 Sensitivity Analysis Results for $\boldsymbol{L_{Amax}}$

relation between noise and the tip speed [7]. On top of that, this relation can be verified in this study via sensitivity analysis between these three design variables and the hovering tip Mach number of rotors, $\boldsymbol{M_{tip,hover}}$. As in Figure 12., when $\boldsymbol{\theta_{0,rotor}}$ increases, $\boldsymbol{M_{tip,hover}}$ decreases and even though $\boldsymbol{GW}$ increases as $\boldsymbol{\theta_{0,rotor}}$ increases, thus enlarging sectional loading on the rotor blade, the increase of $\boldsymbol{M_{tip,hover}}$ overwhelms enlarged sectional loading, therefore $\boldsymbol{L_{Amax}}$ decreases. Likewise, as the absolute magnitude of $\boldsymbol{\theta_{tw,rotor}}$ decreases (less twisted), the average sectional twist angle increases, thus reducing $\boldsymbol{M_{tip,hover}}$. And It finally causes the drop in $\boldsymbol{L_{Amax}}$ in spite of the increase of sectional loading caused by surging $\boldsymbol{GW}$. Lastly, as $\boldsymbol{R_{rotor}}$ increases, $\boldsymbol{M_{tip,hover}}$ decreases. And enlarged sectional loading caused by the increase of $\boldsymbol{GW}$ and expansion of thickness noise sources due to the increase of $\boldsymbol{R_{rotor}}$ are overwhelmed by the reduction in $\boldsymbol{M_{tip,hover}}$, thus causing drop in $\boldsymbol{L_{Amax}}$.

Since in this study, only maximum value of A-weighted OASPL is considerd as noise impact of eVTOL aircraft, noise contours for three designs (*Design A, B and C*) are depicted in Figure 14. In addition, sectional loading distribution around rotor blades for each design is portrayed in Figure 14. And Table 3 explains QoIs of each design.

Table 3. QoIs of Each Design

QoIs	Design A	Design B (baseline)	Design C
$\boldsymbol{GW}$ [lb]	2734	2966	3588
$\boldsymbol{L_{Amax}}$[dBA]	85.89	78.42	70.09
$\boldsymbol{M_{tip,hover}}$	0.64	0.6	0.55

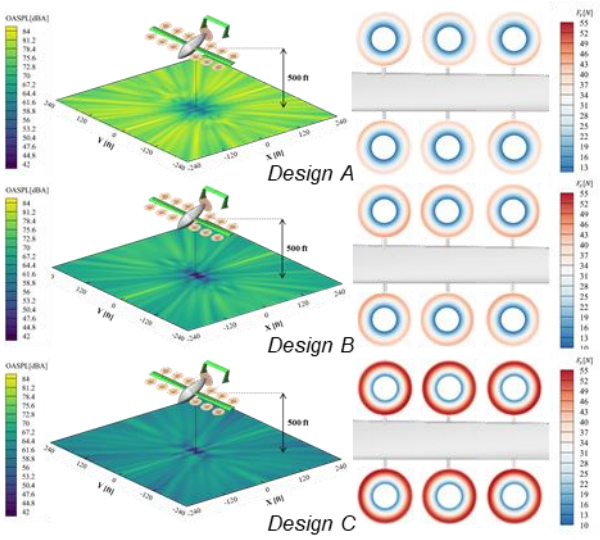

Figure 14 Noise Contour and Lift Distribution for Each Design

As it can be seen in Figure 14, when a design changes from *Design A* to *Design C*, not only $\boldsymbol{L_{Amax}}$ drops from 85.89 dBA to 70.09 dBA, but also overall OASPL on the ground decreases. Furthermore, as mentioned above, even though lift around rotor blades is larger in *Design C* than in *Design A* due to larger $\boldsymbol{GW}$ (3588 lb > 2734 lb), higher $\boldsymbol{M_{tip,hover}}$ (0.64 > 0.55) in *Deisgn A* overwhelms it, thus making *Deisgn A* have poor aeroacoustic performance.

Through ANOVA and sensitivity analysis, design variables which are dominant in determining $\boldsymbol{GW}$ and $\boldsymbol{L_{Amax}}$ are identified. Among these design variables, $\boldsymbol{\theta_{0,rotor}}$, $\boldsymbol{\theta_{tw,rotor}}$ and $\boldsymbol{R_{rotor}}$ show opposite correlations for $\boldsymbol{GW}$ and $\boldsymbol{L_{Amax}}$. That is, these two design variables show positive correlations with $\boldsymbol{GW}$ and negative correlations with $\boldsymbol{L_{Amax}}$ and this will be validated again through the optimization process in Section 6.

6. DESIGN OPTIMIZATION

Using this framework, a global design optimization was conducted on a eVTOL aircraft with the lift+cruise configuration. In this study, the design varaibles and the target payload in Table 2 that were used in the pramatric design study were used agian in the global design optimization.

Next, the genetic algorithm (GA) was selected as an algorithm for the global design optimization and the optimization was conducted on the surrogate model constructed on Section 5.2. GA was adapted since it has advantage of showing good performance for problems with discontinuity and multimodality [25]. Especially, nondominated sorting genetic algorithm II (NSGA-II) was adapted because this algorithm was proved to have good ability of finding Pareto solution set for multiobjective opmization problems by using non-dominated sorting and crowding distance sorting strategies [26]. The opimization process including the GA algorithm was conducted using pymoo library in Python, which is developed for solving optmization problems with multi objective genetic algorithm [27].

Constratins were set to acheive a realistic desgin of the eVTOL aircraft, and $\boldsymbol{GW}$ and $\boldsymbol{L_{Amax}}$ were set as objective functions. Constraints and objective functions are in Table 4. Feasibility in the list of constraints means wheter a design can satisfy the target payload or not, and this is determined based on the surrogate model constructed on Section 5.2 using GPC.

Table 4 Constraints and Objectives

Constraints	Rotor-rotor clearance	> 10 % of the rotor radius
	Rotor-wing clearance	> 10 % of the rotor radius
	$\boldsymbol{M_{tip,rotor}}$	< 0.65
	$\boldsymbol{M_{tip,prop}}$	< 0.8
	Feasibility in terms of payload	
Objectives	$\boldsymbol{GW}$	
	$\boldsymbol{L_{Amax}}$	

Through the optimization process, 353 Pareto solutions were obtained as shown in Figure 15. In addition to Preto points, each point's five most influential design parameters acquired in Section 5.2. ($\boldsymbol{\theta_{0,rotor}}$, $\boldsymbol{\theta_{tw,rotor}}$, $\boldsymbol{R_{rotor}}$, $\boldsymbol{R_{prop}}$ and $\boldsymbol{RPM_{prop}}$) are shown in Figure 14 where each parameter is normalized.

As in Figure 15, a clear trade-off relation between $\boldsymbol{GW}$ and $\boldsymbol{L_{Amax}}$ is shown. In addition, as a design change from n = 1 to n = 353, which corresponds to $\boldsymbol{L_{Amax}}$ being reduced and $\boldsymbol{GW}$ being surged, $\boldsymbol{\theta_{0,rotor}}$ increases, $\boldsymbol{R_{rotor}}$ increases, and $\boldsymbol{\theta_{tw,rotor}}$ decreases. This is in accordance with the results from the parametric study. In Section 5.2. it was validated that these design variables have significant influences in deciding $\boldsymbol{GW}$ and $\boldsymbol{L_{Amax}}$,and they have opposite correlations

between these two objectives; these relations are revalidated through the optimization process. On the other hand, $\boldsymbol{R_{prop}}$ and $\boldsymbol{RPM_{prop}}$ remain almost same from n = 1 to n = 353, and again this is a revalidation of the results from the parametric study. Through the paramteric study, it was shown that $\boldsymbol{R_{prop}}$ and $\boldsymbol{RPM_{prop}}$ have strong influences only on $\boldsymbol{GW}$, and as in Figure 15, these two design varaibles barely change across Pareto solution sets.

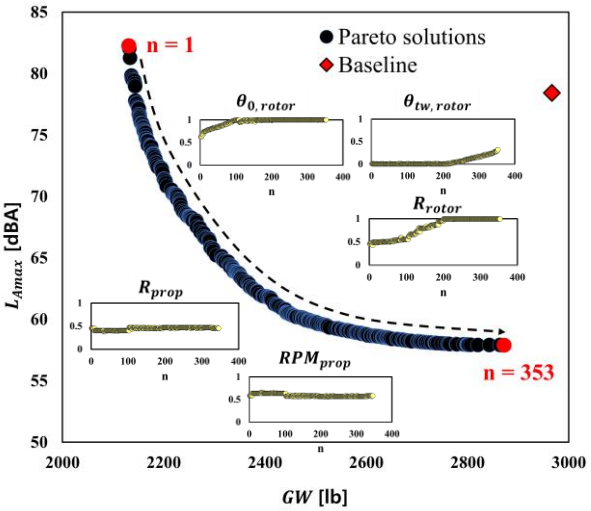

Figure 15 Pareto Solutions Obtained Based on Surrogate Model

7. CONCLUSION

In this study, a design methodology of UAM vehicles for noise mitigation at a conceptual design stage was newly developed. In the new design methodology, a flight analysis module using RISPECT+ & CAMRAD II coupling was used to predict aerodyanmic force distribution accurately, therefore accurate noise prediction is possible. In addition, for fast noise calculation at the conceptual design stage, noise prediction module with compact loading assumption and dual compact loading assumption was used. By using this noise mudule, noise impact of an eVTOL aircraft can be evaluated in a short time. Using the new methodology, parametric study and design optimization were conducted and physical insights of desigining eVTOL aircraft when considering both the gross weight and noise impact were acquired.

First, design variables related with hovering performance have opposite correlations for the hovering tip Mach number and gross weight of eVTOL aircraft. Second, even though tip Mach number and gross weight change in opposite directions, the effect on noise impact by the tip Mach number change overwhelms that by the gross weight change. Finally, because of the two reasons just mentioned, the gross weight and the noise impact have trade-off relation when desigining eVTOL aircraft.

As a future work, validation and improvement of CAMRAD II model using computation fluid dynamics (CFD) simulations is being considered. By conducting validation and improvemnet procedure, it is expected that the methodology becomes more accurate and realistic.

ACKNOWLEDGEMENT

This research was supported by Unmanned Vehicles Core Technology Research and Development Program through the National Research Foundation of Korea(NRF) and Unmanned Vehicle Advanced Research Center(UVARC) funded by the Ministry of Science and ICT, the Republic of Korea (2020M3C1C1A02081911)

REFRENCES

[1] Holden, J., Goel, N., “Fast-Forwarding to a Future of On-Demand Urban Air Transportation,” Uber Inc., San Francisco, CA, 2016, pp. 1–98.

[2] Heineke, K., Kloss, B., Riedal, “The future of air mobility: Electric aircraft and flying taxis,” McKinsey&Company, November 2021.

[3] Lee, S., Ko, B., Ahn, S., Hwang, H., “Initial Sizing of a Tilt Ducted Fan Type eVTOL for Urban Air Mobility,” Journal of Korean Society for Aviation and Aeronautics, Vol. 29, No. 3, 2021, pp. 52-65.

[4] Rizzi, S., “Urban Air Mobility Noise: Current Practice, Gaps, and Recommendations,” NASA Technical Report, 2020, pp. 1-48.

[5] Maurice, L., Lee, D., “Assessing Current Scientific Knowledge, Uncertainties and Gaps in Quantifying Climate Change Noise and Air Quality Aviation Impacts,” Final Report of the International Civil Aviation Organization (ICAO) Committee on Aviation and Environmental Protection (CAEP) Workshop, US Federal Aviation Administration and Manchester Metropolitan University, Washington DC and Manchester, 2009, pp. 1-53.

[6] Chae, S., Yee, K., Yang, C., Aoyama, T., Jeong, S., Obayashi, S., “Helicopter Rotor Shape Optimization for the Improvement of Aeroacoustic Performance in Hover,” Journal of Aircraft, Vol. 47, No. 5, October 2010, pp. 1770-1783.

[7] Hong, Y., Han, D., Yee, K., “Design Parameter Study of Drone Blade Considering Aeroacoustics,” 31st Congress of the International Council of the Aeronautical sciences, September 09-14, 2018

[8] Faulkner, H., “The Cost of Noise Reduction in Intercitiy Commercial Helicopters,” Journal of Aircraft, Vol. 11, No. 2, Feburary 1974, pp. 89-95.

[9] Johnson, W., “Technology Drivers in the Development of CAMRAD II,” American Helicopter Society Aeromechanics Specialist Meeting, San Francisco, California, January 1994.

[10] Lee, D., Lim, D., Yee, K., “Generic Design Methodology for Vertical Takeoff and Landing Aircraft with Hybrid-Electric Propulsion,” Journal of Aircraft, Vol. 59, No. 2, August 2021.

[11] Lee, D., and Yee, K., “Advanced Analysis Method of Electric Propulsion System for UAM Vehicles,” *Proceedings of the 47th European Rotorcraft Forum*, Sept. 7–9, 2021, Virtual.

[12] Liu, Q., “Analysis, design and control of permanent magnet synchronous motors for wide-speed operation,” Ph.D. Dissertation, National University of Singapore, 2005.

[13] Hassan, W., Wang, B., “Efficiency optimization of PMSM based drive system,” Proceedings of the 7th International Power Electronics and Motion Control Conference, Vol. 2, June 2012, pp. 1027-1033.

[14] Mestha, L., Evans, P., Analysis of on-state losses in PWM inverters. Electric Power Applications,” IEEE Proceedings B, Vol. 136, No.4, 1989, pp.189–195.

[15] Misra, A., “Summary of 2017 NASA Workshop on Assessment of Advanced Battery Technologies for Aerospace Applications,” NASA Glenn Research Center Report, Cleveland, Ohio, January 2018, pp. 1–18.

[16] Lee, D., Kang, S., and Yee, K., “A Comparison Study of Rotorcraft with Hybrid Electric Propulsion System,” Proceedings of the 45th European Rotorcraft Forum, Warsaw, Poland, September 17–20, 2018.

[17] Farassat, F., Brentner, K., “The Acoustic Analogy and the Prediction of the Noise of Rotating Blades,” Theoretical and Computational Fluid Dynamics, Vol. 10, 1997, pp. 155-170.

[18] Brentner, K., Jones, H., “Noise Prediction for Maneuvering Rotorcraft,” AIAA Aeroacoustics Conference, Hampton, Virginia, June 12-14, 2000.

[19] Yang, T., Brentner, K., Walsh, G., “A Dual Compact Model for Rotor Thickness Noise Prediction”, American Helicopter Society Journal, Vol. 63, No. 2, April 2018, pp. 12-23.

[20] Brentner, K., Farassat, F., “Modeling Aerodynamically Generated Sound of Helicopter Rotors, ” Progress in Aerospace Science, Vol. 39, 2003, pp. 83-120.

[21] Vegh, J., Botero, E., Clarke, M., Trent, J., Alonso, J., “Current Capabilities and Challenges of NDARC and SUAVE for eVTOL Aircraft Design and Analysis,” AIAA Propulsion and Energy 2019 Forum, AIAA Paper 2019-4505, Aug. 2019.

[22] McKay, M., Beckman, R., Conover, W., “A Comparison of Three Methods for Selecting Values of Input Variables in the Analysis of Output from a Computer Code,” American Statistical Association, Vol. 21, No. 2, May 1979, pp. 239–245

[23] Rasmussen, C., Williams, K., “Gaussian Processes for Machine Learning,” the MIT Press, 2006.

[24] Sobol, I., “Global Sensitivity Indices for Nonlinear Mathematical Models and Their Monte Carlo Estimates,” Mathematics and Computers in Simulation, Vol. 55, No. 1, February 2001, pp. 271-280.

[25] Sasaki, D., Obayashi, S., “Efficient Search for Trade-Offs by Adaptive Range Multi-Objective Genetic Algorithms,” Journal of Aerospace Computing, Information and Communication, Vol. 2, No. 1, January 2005, pp. 44–64.

[26] Deb, K., Pratap, A., Agarwal, S., Meyarivan, T., “A Fast and Elitist Multiobjective Genetic Algorithm : NSGA-II,” IEEE Transactions on Evolutionary Computation, Vol. 6, No. 2, April 2002, pp. 182-197.

[27] Blank, J., Deb, K., “pymoo: Multi-Objective Optimization in Python,” IEEE Access, Vol. 8, 2020, pp. 89497-89509

APPENDIX

A1. Cross-Validation results